Design and Modeling of Hybrid Electric Vehicle Powered by Solar and Fuel Cell Energy with Quadratic Buck/Boost Converter

G. DIVYA[1,2], VENKATA PADMAVATHI S.[1]
[1]GITAM School of Technology, GITAM Deemed to be University, Hyderabad, Telangana, INDIA
[2]CVR College of Engineering, Hyderabad, Telangana, INDIA

Abstract: - Considering technological advancements and international standards mandating reduced greenhouse gas emissions, automobile manufacturers have shifted their focus toward innovative technologies related to fuel-cell electric vehicles. Despite having an all-electric powertrain, fuel cell electric vehicles (FCEVs) utilize a fuel cell stack as their energy source, which runs on hydrogen and results in the emission of only water and heat. Due to the absence of tailpipe pollutants, fuel-cell electric vehicles are considered zero-emission vehicles. Among fuel cell types, low-temperature and low-pressure fuel cells, such as Proton Exchange Membrane Fuel Cells (PEMFCs), are well-suited for vehicular applications as they exhibit high power density, operate at lower temperatures (60-80°C), and are less prone to corrosion than other types of fuel cells. The main objective of this paper is to investigate solar-assisted electric fuel cell vehicles that efficiently integrate the fuel cell system with an electrolyzer and solar power to fulfill the fluctuating power demands of the electric motor and auxiliary systems. A novel EV configuration with a fuel cell, electrolyzer and onboard PV cell is proposed. An onboard PV cell can assist the fuel cell when the irradiation is enough to generate the power. During the idle conditions of vehicles, PV-generated power can be converted into chemical energy using an electrolyzer and generated hydrogen can be stored in a hydrogen tank. To match the voltage required by the motor and sources a quadratic bidirectional buck-boost converter is employed. The proposed configuration is examined by considering variable irradiance and variable speed values. To obtain the maximum power output from the photovoltaic (PV) panel, a Maximum Power Point Tracking (MPPT) algorithm is employed to regulate the PV system. To enhance the efficiency and cost-effectiveness of PV systems, an enhanced version of the incremental conductance algorithm is utilized as the MPPT control strategy. Outer voltage and inner current control are adopted to regulate the DC output voltage of the QBBC converter. An indirect vector-controlled induction motor is used as vehicle drive. Simulations are performed to investigate the proposed EV configuration in MATLAB/SIMULINK.

Key-Words: - QBBC, Hybrid Electric Vehicle, PV generation, MPPT, Fuel Cell, Induction Motor, Vector Control

Received: April 19, 2022. Revised: March 13, 2023. Accepted: April 14, 2023. Published: May 8, 2023.

1 Introduction

During the 20th century's early days of transportation, there existed a spirited competition between electrically powered automobiles and those with internal combustion engines (ICEs). The internal combustion engine emerged victorious, mainly because liquid fuels store a significant amount of energy, enabling automobiles to travel long distances without the need for frequent refueling. In comparison, approximately 28 kilograms of thirty liters of fuel contain around 250 kWh of energy, whereas a lithium-ion battery weighing the same 28 kilograms only provides about 5 kWh of energy, [1]. The undeniable energy advantage of liquid fuel has ensured the dominance of the internal combustion engine for the past century, despite its relatively low efficiency. The drawbacks of utilizing internal combustion engines and fossil fuels are well anticipated, such as decreased efficiency, air pollution, reliance on fossil fuels, dependence on foreign oil, and lead poisoning. Over the years, various alternatives to the gasoline-powered internal combustion engine have been proposed to combat these issues, including steam power, turbine engines, electric vehicles, and the utilization of alternative fuels such as methanol, ethanol, compressed natural gas, and propane. While fuel cell electric vehicles powered by hydrogen were developed in the mid-90s, it was not until after

2010 that their widespread commercial availability increased, [2].

In a fuel-cell hybrid electric vehicle, the main power source is a fuel cell stack, which is accompanied by a supplementary energy storage system used to power the vehicle's electric motor, [3]. Compared to conventional hybrid electric vehicles or those based on internal combustion engines (ICEs), fuel-cell hybrid electric vehicles have several advantages. The utilization of an electric motor instead of a petrol or diesel-powered ICE improves efficiency and minimizes environmental impacts, making them a more sustainable option, [4]. In a plug-in hybrid electric vehicle (PHEV), an internal combustion engine (ICE) is utilized to increase the vehicle's travel range, [5]. It also generates the electric power required to power the vehicle's electric motor when the battery level reaches a predetermined state of charge (SOC), [6]. Fuel cell hybrid electric vehicles offer several advantages, such as increased efficiency, reduced air pollution, utilization of clean and cost-effective energy resources, and suitability for various industrial applications, [7], [8], [9]. An FC stack generates electric power through a chemical reaction that occurs in the presence of hydrogen, oxygen, and an electrolyte. Among the various FC systems available, the proton exchange membrane FC technology is the most suitable for use in vehicles due to its higher density in electric power generation and reduced heat generation, which improves overall efficiency, [10].

The primary disadvantage of using an FC stack in a vehicle is its inability to respond adequately to sudden changes in the vehicle's load demand, [11]. The FC stack is not capable of responding effectively to sudden increases and decreases in power demand, such as those required during acceleration and deceleration, or the significant initial power needed to start the vehicle, [12]. An additional drawback is that the FC stack itself is unable to store the regenerated power produced during braking and deceleration, thereby necessitating the use of an electrolyzer.

In this paper, a novel EV configuration with a fuel cell, electrolyzer, and onboard PV cell is proposed. An onboard PV cell can assist the fuel cell when the irradiation is enough to generate the power. During the idle condition of the vehicle, PV-generated power can be converted into chemical energy using an electrolyzer and generated hydrogen can be stored in a hydrogen tank. To match the voltage required by the motor and sources a quadratic bidirectional buck-boost converter is employed. The proposed configuration is examined by considering variable irradiance and variable speed values. Section 2 is explained about proposed EV configuration and fuel cell and electrolyzer. Section 3 is about the indirect vector control of the induction motor. The model outcome is shown in Section 5.

2 Proposed Electric Vehicle with Solar Onboard

The need for Continuous power requires the use of equipment with an energy storage system, which raises the cost and reduces reliability. In a nutshell, solar energy and fuel cells are regarded as efficient and environmentally friendly power generation methods in the twenty-first century. Both solar energy and fuel cells have benefits and drawbacks. The proficiency and consistency of Hybrid Electric Vehicles (HEV) can be adjusted by combining their advantages. Figure 1 depicts a typical electric vehicle structure with solar and fuel cells. Moreover, Figure 2 presents an HEV with a Solar and a Fuel Cell.

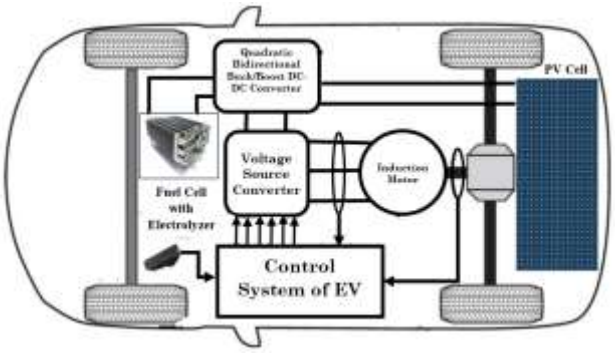

Fig. 1: Outline of Hybrid Electric Vehicle

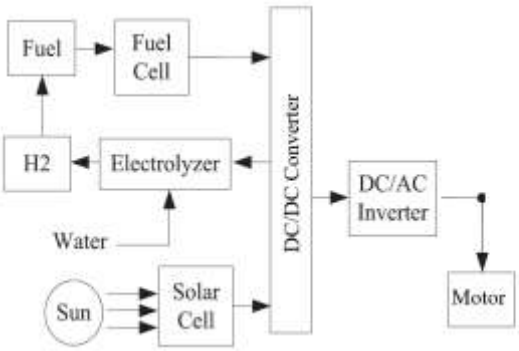

Fig. 2: HEV with Solar and Fuel Cell

HEVs utilize DC-DC bidirectional boost-buck converters that enable power to flow in both

directions. High-gain boost converters have emerged as a hot research topic in power electronics due to their increasing demand in various fields, including fuel cell systems, distributed photovoltaic generation systems, and uninterruptable power supply systems. Applications such as fuel cell systems, distributed photovoltaic generation systems, and uninterruptable power supply systems require a relatively high gain, Vout/Vin (where Vout is the output voltage and Vin is the input voltage), which has made the development of high-gain boost converters a hot research topic in power electronics. However, conventional boost converters have limitations, such as the need for an extremely small off-time for the switch, high-voltage stresses on the switches, and low efficiency, making it challenging to achieve such a high step-up gain. As a result, there is a need for high-gain, high-efficiency converters that do not have the limitations mentioned above.

By adjusting the duty cycle or increasing the turns ratio of the coupled inductor, the voltage gain of a converter can be increased. However, many of these converters suffer from significant input current ripple. One alternative approach is the use of quadratic converters, which have gained increasing attention among power electronics researchers as they can also increase the voltage gain of conventional boost converters.

2.1 Electrolyzer

The Unipolar Stuart cell is a reliable and robust cell that is both low maintenance and highly efficient. This cell produces either H2 (cathode) or O2 (anode) from each electrode's single polarity. The electrolyzer is composed of numerous cells that are separated from one another within separate cell compartments. The electrolyzer enables circulation of the electrolyte through the channels between the electrodes and cell separator by utilizing the H2 and O2 gases that rise in those channels. The cell voltage, which typically ranges from 1.7 to 1.9 V, is maintained under normal operating conditions. The material constraints in the electrolyzer are reduced as its operating temperature does not exceed 70°C. The H2 produced has a purity of 99.9%. Additionally, the current efficiency is 100%, resulting in a hydrogen production rate of:

$$X_{H_2} = 5.18e^{-6} I_e mole/s \quad (1)$$

The current between electrodes is represented by Ie, and the produced H2 is stored in a tank at 3 bar pressure. This stored hydrogen is utilized to supply the load power when the insolation levels are low and the fuel cell needs to be fed.

2.2 Fuel Cell

The system design should consider an important factor that affects the electrolysis process. It is important to note that when the electrolyzer current reaches zero, it is necessary to maintain a protective voltage to prevent excessive corrosion of the cathodic potentials. The proposed electric storage device is designed to address this issue by isolating the electrolyte from the electrolysis cell and introducing N2 into the electrolyzer. This helps to protect the electrodes from corrosion when the electrolyzer current drops to zero[13].

The system proposed utilizes air as the oxidant and maintains a cell pressure at atmospheric conditions with a temperature of 70°C. The electrical performance of the fuel cell is related to the state variables by the Nernst equation at atmospheric pressure, considering the current density designed as 400 mA/cm2, which requires the use of 90 fuel cells in a stack.

$$V_o = E_o + \frac{R.T}{2F} \ln \frac{x_{H_2} x_{O_2}{}^{0.5}}{x_{H_2O}} \quad (2)$$

A detailed description of a PV generation system with incremental conductance-based MPPT and fuel cell with a DC-DC converter is presented in [14].

2.3 Quadratic Bidirectional Boost /Buck DC-DC Converter

Figure 1 illustrates the power topology of the Quadratic Bidirectional Boost/Buck DC-DC converter. Unlike the classical Boost quadratic converter, this topology does not require additional passive components such as inductors and capacitors. Additionally, it features a fixed voltage gain with a quadratic function for both Boost and Buck modes of operation. Furthermore, the charging or discharging of the converter depends only on a single transistor. To investigate, the bidirectional DC/DC converter will be assumed to be in steady-state operation. The power converter operates in two different modes: The bidirectional DC/DC converter operates in two modes: Boost mode and Buck mode. In Boost mode, the converter transfers energy from the input side to the output side. During this mode, two IGBTs (T1 and T4) remain in the OFF state, while IGBT T3 remains in the ON state. The switching time of T2 can be controlled using PWM with an output voltage control and inner current control.

During Boost mode, the bidirectional DC/DC converter operates by transferring energy from the input side to the output side. The IGBTs T1 and T4 remain in the OFF state, while IGBT T3 remains in the ON state. The switching time of T2 is controlled by pulse width modulation (PWM) with a time interval of ΔTs, which can be adjusted using output voltage control and inner current control. When T2 is in the ON state, the inductors L1 and L2 are charged with a linearly increasing current, transferring energy stored in the capacitor C to the inductor L2. When T2 is in the OFF state, the inductors L1 and L2 are discharged with a linearly decreasing current, transferring energy stored in the inductors to the capacitor and output side.

$$\Delta V_{in} + (1-\Delta)(V_{in} - V_c) = 0 \quad (3)$$
$$\Delta V_c + (1-\Delta)(V_c - V_{out}) = 0 \quad (4)$$

Then voltage gain is given as

$$G = \frac{V_{out}}{V_{in}} = \frac{1}{(1-\Delta)^2} \quad (5)$$

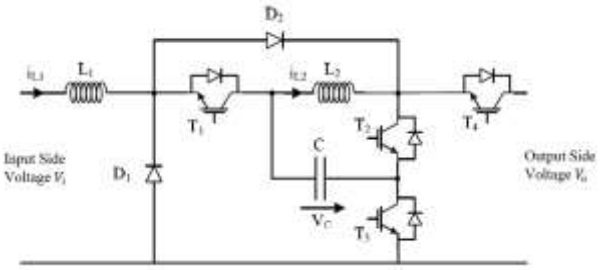

Fig. 3: Quadratic bidirectional boost /buck DC-DC Converter

When the converter operates in reverse mode, it transfers energy from the output side to the input side and is categorized as a Buck converter. The IGBTs T_2 and T_3 are always in the OFF state and the IGBT T_4 is always in the ON state. PWM with altering the time of T_c can be applied to T_1 using output voltage control and inner current control. When T_1 is in ON state (in the time interval of ΔT_s) the flows in inductors L_1 and L_2 will increase linearly as capacitor C is discharging since its energy will be transferred to inductor L_1. When T_1 is in the OFF state (during the time interval of 1-ΔTs), the currents in the inductors L_1 and L_2 will decrease linearly and During the Buck mode of operation, the energy that was previously stored in the inductors L1 and L2 is transferred to the capacitor C and the input side of the converter. During Buck Mode

$$\Delta(V_c - V_{in}) - (1-\Delta)V_{in} = 0 \quad (6)$$
$$\Delta(V_c - V_{out}) + (1-\Delta)V_c = 0 \quad (7)$$

Then voltage gain is given as

$$G = \frac{V_{in}}{V_{out}} = \Delta^2 \quad (8)$$

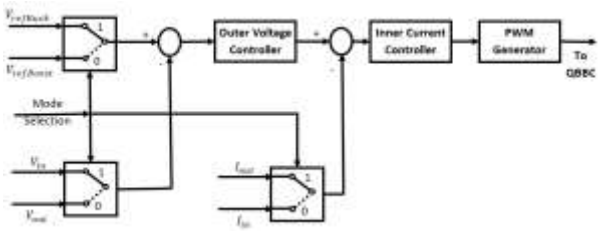

Fig. 4: Control Strategy for QBBC

The controlling strategy for the bidirectional DC-DC converter is presented for both buck and boost modes in Figure 3. Depending on power flow or current direction, mode selection selects the converter to work as buck mode or boost mode. Controlling of a DC-DC converter comprises an outer voltage control loop for voltage regulation and the proposed converter has several advantages, including the use of an inner current control loop for precise current regulation and the use of PI controllers for both voltage and current regulation.

1. The proposed converter is suitable for low-to-medium power applications due to its low input current ripple and low conduction loss.
2. The proposed converter provides a significantly higher step-up voltage gain than a traditional quadratic boost converter.
3. The proposed converter also experiences significantly lower voltage stresses on its main switch and diodes compared to a traditional quadratic boost converter at the same output voltage, which can contribute to improved reliability and longer operating lifetimes.

3 Indirect Vector Control of Induction Motor for Electric Vehicle

Induction motor is chosen as electric vehicle drive due to their reliability for dynamic conditions, simple construction, ruggedness, minimum service requirement, and commercial moderation. Due to the absence of brushes, friction losses are reduced and it's possible to rise restrictions for probable maximum speed. High-output mechanical power is possible to increase maximum speed. The frequency of input voltage can be altered to change the speed of the motor or vehicle.

The vector control of an induction machine involves predicting the position of the rotor flux linkage phasor, denoted as λ_r. A phasor diagram depicting

the vector control is presented in Figure 4, where λ_r is located at an angle of θ_f with respect to the stationary reference. Here, θ_f represents the field angle.

The three-phase stator currents can be transformed into q and d axes currents in the synchronous reference frames by using Park transformation.

$$\begin{bmatrix} i_{qs} \\ i_{ds} \end{bmatrix} = \frac{2}{3}\begin{bmatrix} \cos\theta_f & \cos\left(\theta_f - \frac{2\pi}{3}\right) & \cos\left(\theta_f + \frac{2\pi}{3}\right) \\ \sin\theta_f & \sin\left(\theta_f - \frac{2\pi}{3}\right) & \sin\left(\theta_f + \frac{2\pi}{3}\right) \end{bmatrix} \quad (9)$$

$$|i_s| = \sqrt{(i_{qs})^2 + (i_{ds})^2} \quad (10)$$

and the stator phase angle is

$$\theta_s = \left(\frac{i_{qs}}{i_{ds}}\right) \quad (11)$$

where i_{qs} and i_{ds} The 'q' and 'd' axes currents in the synchronous reference frame are obtained by projecting the stator current phasor on the 'q' and 'd' axes, respectively. It is important to note that the current phasor magnitude remains constant regardless of the chosen reference frame.

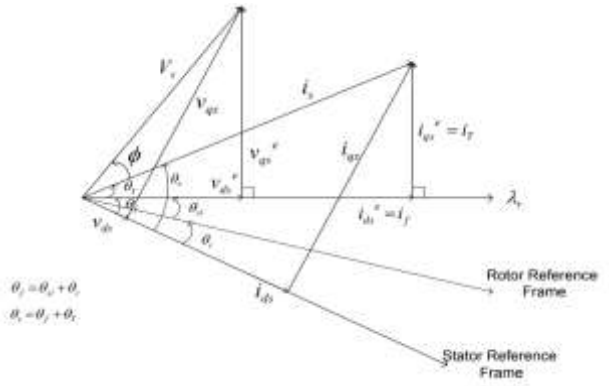

Fig. 5: Phasor representation of stator and rotor quantities

The rotor flux λ_r and torque T_e are produced by the stator's current i_s. To ensure that the current component responsible for producing the rotor flux is in phase with λ_r , the stator current phasor is resolved along λ_r , revealing the field-producing component i_f. The torque-producing component i_T is then identified as the perpendicular component to

$$i_f \quad . \quad \lambda_r \propto i_f \quad (12)$$

$$T_e \propto \lambda_r i_T \propto i_f i_T \quad (13)$$

In a steady state, the components i_f and i_T become only DC components as their relative speed with respect to the rotor field is zero.

By considering the synchronous reference frame, the orientation of λ_r is determined, allowing the flux and torque-producing components of currents (i_f and i_T) to be considered as dc quantities that can be used as control variables. Till now it was assumed that the rotor flux position is available, but it has to be obtained at every instant. This field angle can be written as,

$$\theta_f = \theta_{sl} + \theta_r \quad (14)$$

where θ_r is the rotor position and θ_{sl} is the slip angle. In terms of the speeds and time, the field angle can be written as

$$\theta_f = \int(\omega_r + \omega_{sl})dt = \int(\omega_s)dt \quad (15)$$

Vector control schemes can be categorized as direct and indirect vector control schemes, depending on the method used to determine the instantaneous rotor flux position. Direct vector control schemes calculate the field angle using terminal voltages and currents, Hall sensors, or flux-sensing windings. In contrast, indirect vector control schemes obtain the rotor flux position using rotor position measurement and partial estimation with only machine parameters, without relying on other variables such as voltages and currents.

The indirect vector control scheme assumes a current source inverter, in which case the stator phase currents serve as inputs, allowing for the neglect of stator dynamics. The dynamic equations for the induction motor in the synchronous reference frame can then be derived, with the rotor flux taken as the state variable. These equations can be expressed as:

$$r_r i_{qr} + \frac{d\lambda_{qr}}{dt} + \omega_{sl}\lambda_{dr} = 0 \quad (16)$$

$$r_r i_{dr} + \frac{d\lambda_{dr}}{dt} - \omega_{sl}\lambda_{qr} = 0 \quad (17)$$

Where

$$\omega_{sl} = \omega_s - \omega_r \quad (18)$$

$$\lambda_{qr} = L_r i_{qr} + L_m i_{qs} \quad (19)$$

$$\lambda_{dr} = L_r i_{dr} + L_m i_{ds} \quad (20)$$

If the resultant rotor flux linkage, λ_r , also known as the rotor flux linkages phasor, is aligned with the direct axis, and the induction motor achieves field orientation. This alignment reduces the number of variables that need to be considered. Aligning the d-axis with the rotor flux phasor results in

$$\lambda_r = \lambda_{dr} \tag{21}$$

$$\lambda_{qr} = 0 \tag{22}$$

$$\frac{d\lambda_{qr}}{dt} = 0 \tag{23}$$

Then

$$r_r i_{qr} + \omega_{sl}\lambda_r = 0 \tag{24}$$

$$r_r i_{dr} + \frac{d\lambda_{dr}}{dt} = 0 \tag{25}$$

$$i_{qr} = \frac{-L_m}{L_r} i_{qs} \tag{26}$$

$$i_{dr} = \frac{\lambda_r - L_m i_{ds}}{L_r} \tag{27}$$

The equations for the rotor currents in the d and q axes can be written as follows:

$$i_f = \frac{1}{L_m}[1 + T_r P]\lambda_r \tag{28}$$

$$\omega_{sl} = -\frac{r_r i_{qr}}{\lambda_r} = \frac{L_m}{T_r}\frac{i_T}{\lambda_r} \tag{29}$$

Where

$$i_T = i_{qs}, i_f = i_{ds}, T_r = \frac{L_r}{r_r}, K_{te} = \frac{4}{3P} \tag{30}$$

Replacing the rotor currents, the torque is given as

$$T_e = \frac{3P}{4}\frac{L_m}{L_r}\left(\lambda_{dr} i_{qs} - \lambda_{qr} i_{ds}\right) = \frac{3P}{4}\frac{L_m}{L_r}\lambda_{dr} i_{qs} = K_{te}\lambda_r i_{qs} \tag{31}$$

From Equation (31) torque is related to the rotor flux linkages λ_r and the stator q-axis current i_{qs}. That means torque is directly proportional to stator current by making rotor flux linkage to be constant. The stator current phasor is the resultant of the 'd' and the 'q' axes stator currents in any reference frame given as

$$|i_s| = \sqrt{\left(i_{qs}\right)^2 + (i_{ds})^2} \tag{32}$$

The speed of the motor and input currents can be measured and fed back to the indirect vector controller to generate reference currents. The indirect vector control is implemented as illustrated in Figure 5, where the PI controller takes the speed error as its input and generates a reference torque signal. Similarly, the implementation of vector control is presented in Figure 6. Torque reference generated from the PI controller reduces the error between reference speed and actual speed. From the field weakening technique reference flux is calculated from the speed of the motor which is given as

$$\lambda_r^* = \begin{cases} \lambda_b & if\ 0 \le |\omega_r| \le \omega_{rated} \\ \frac{\omega_b}{|\omega_r|}\lambda_b & if\ \omega_b \le |\omega_r| \le \omega_{r(max)} \end{cases} \tag{33}$$

where λ_b is rated rotor flux and ω_r rated rotor speed. Up to rated speed reference flux is met to rated flux and for speed more than valued speed reference flux can be weakened near keep the power output to be constant.

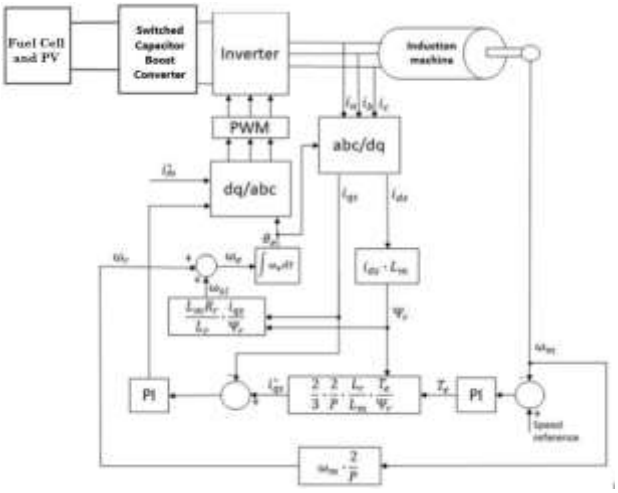

Fig. 6: The implementation of vector control

4 Simulink Model of the Proposed System

The proposed hybrid electric vehicle configuration is modeled in MATLAB/SIMULINK to check the efficiency. The outline of the simulated system is shown in Figure 1. A fuel cell is the main source for the electric vehicle, a rooftop solar cell is considered a secondary source, and regenerative energy during braking or deceleration of the electric vehicle can be stored in a hydrogen tank by converting electrical energy into chemical energy by using an electrolyzer. Indirect vector control is adopted for speed control of vehicle drive. Change in irradiation, change in speed, and change in torque

are considered to simulate the behavior of the proposed configuration. The parameters of the system are depicted in Table 1.

Table 1. Parameters of the System

Induction Motor Parameters	
Nominal Power, voltage, and frequency	50KW, 460V, 50Hz
Stator Resistance and Inductance	87mΩ and 0.8mH
Rotor Resistance and Inductance	228mΩ and 0.8mH
Mutual Inductance	34.7mH
Inertia, Friction Factor, and Pole Pairs	1.662kg.m^2, 0.1N.m.s. and 2
QBBC Parameters	
L_1, L_2 and C	2mH, 15mH and 5µF
PV Array and DC-DC converter Parameters	
Series connected modules and Parallel Strings	2 and 3
V_{oc} and I_{sc}	65.1V and 6.46A
V_{mpp} and I_{mpp}	54.7 and 5.98A
C_{in}, L, and C_{out}	100µF, 70mH and 100µF
Fuel Cell and DC-DC Converter Parameters	
Nominal Voltage and Power	200V and 50KW
L and C_{out}	3mH and 1600µF

CASE 1: In this case, reference speed is increased from 100 rad/sec to 120 rad/sec at 10 seconds with constant irradiation of 1000w/m^2 as shown in Figure 7. The reference speed of the motor in vector control is 100rad/s up to 10 seconds, after that speed is increased to 120rad/s. Motor response with a conventional bidirectional buck-boost converter is presented in Figure 8. Stator currents when speed is increasing from the initial state are shown in Figure 8a. The speed of the motor and electromagnetic torque is indicated in Figure 8 b. Due to limited power, low voltage gain and high current stress will increase the ripples in stator currents and hence speed and torque. The tracking ability of the actual speed of the motor is also very poor as rise time, percentage ripples, and stability time are very high as shown in Figure 8 and Figure 9. With the adopted QBBC converter generated voltage, current, and power from the PV array are shown in Figure 10. PV voltage is boosted up using MPPT operated DC-DC boost converter up to 400V. The incremental conductance algorithm is adopted as MPPT due to its robustness to the variation of atmospheric conditions. With 1000 w/m^2 irradiation, generated power from the PV cell is 2.01 KW. Figure 11 displays the output voltage, current, and power of the PV converter. The voltage, current, and power generated by the fuel cell are illustrated in Figure 12, while Figure 13 shows the voltage, current, and power of the fuel cell converter.

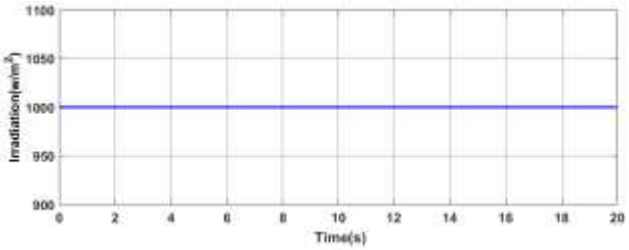

Fig. 7: Irradiance of PV cells

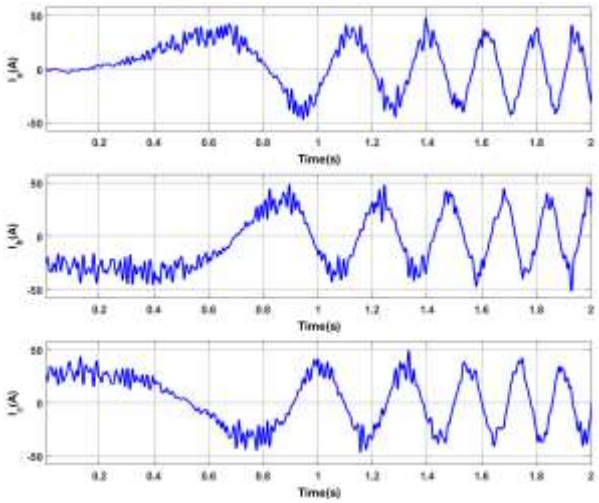

Fig. 8: Response of Induction motor currents with conventional Bidirectional Buck Boost converter

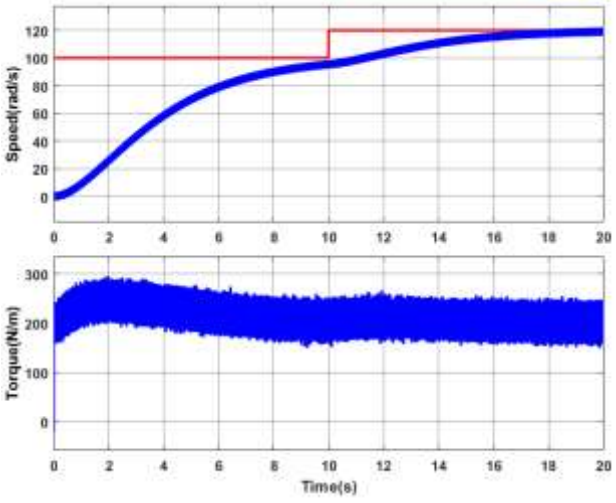

(b)

Fig. 9: Response of Induction motor Speed and Torque with conventional Bidirectional Buck Boost converter

The voltage, current, and power of the electrolyzer are represented in Figure 14 and Figure 15. Additionally, Figure 16 presents the input and output voltages of the QBBC converter. input voltage of 400V is boosted to 780V, which is required by vehicle drive, by the QBBC converter by using voltage and current loops. The speed of the vehicle drive and its torque are shown in Figure 17 and input three-phase stator currents are shown in Figure 18.

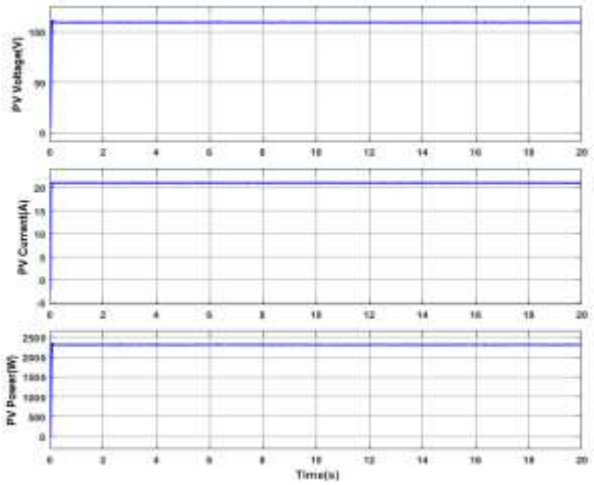

Fig. 10: PV array output voltage, current, and power

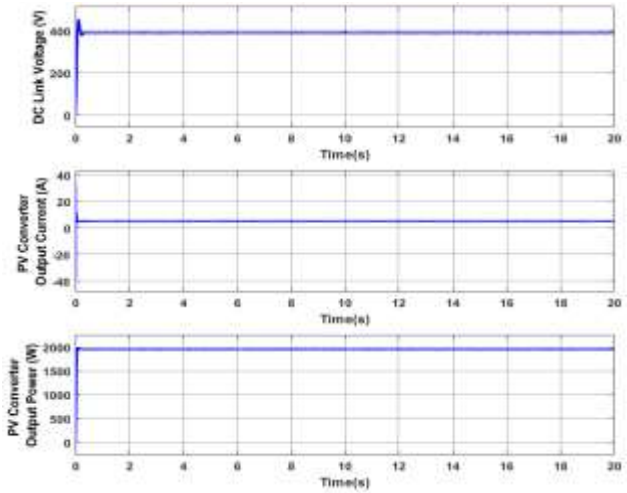

Fig. 11: PV converter output voltage, current, and power

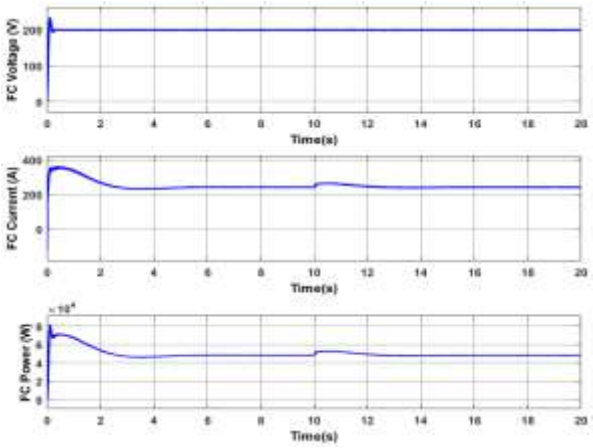

Fig. 12: Fuel Cell output voltage, Current, and power

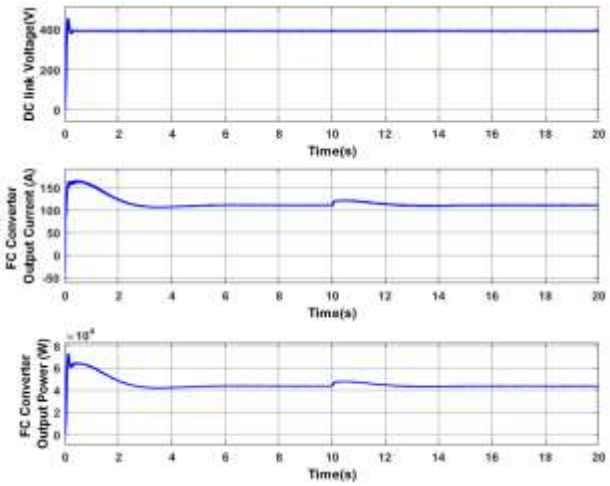

Fig. 13: Fuel Cell converter output voltage, current, and power

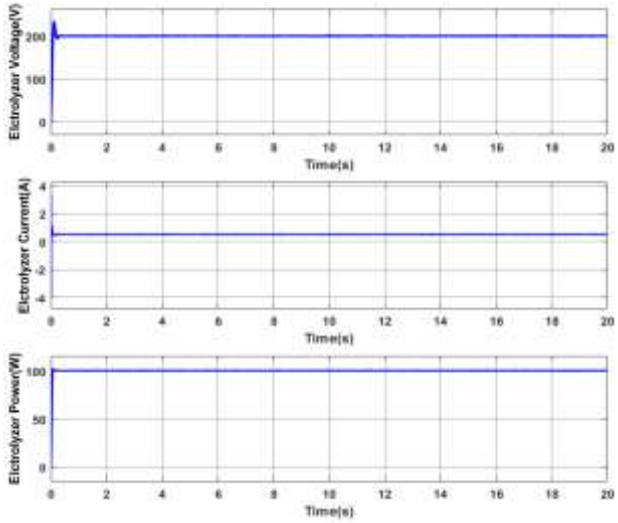

Fig. 14: Electrolyzer output voltage, current, and power

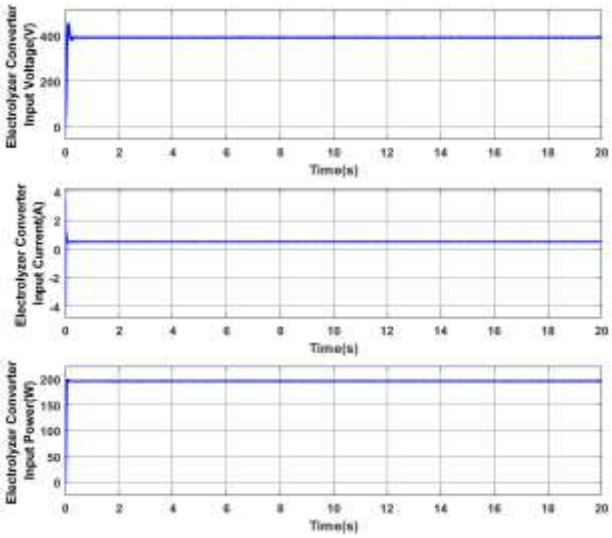

Fig. 15: Electrolyzer converter input voltage, current, and power

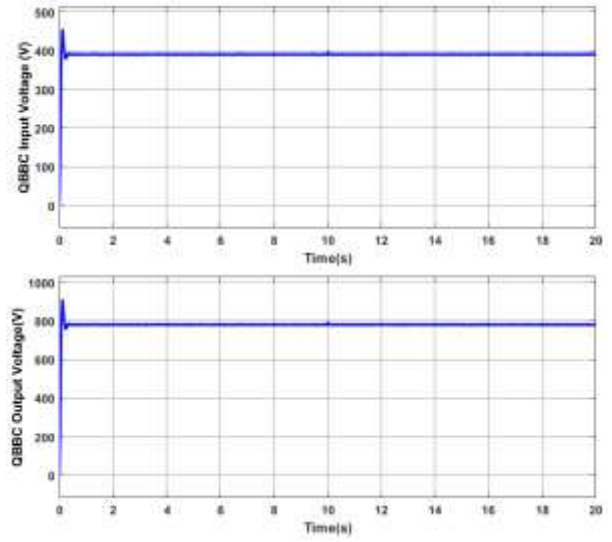

Fig. 16: QBBC input voltage and output voltage

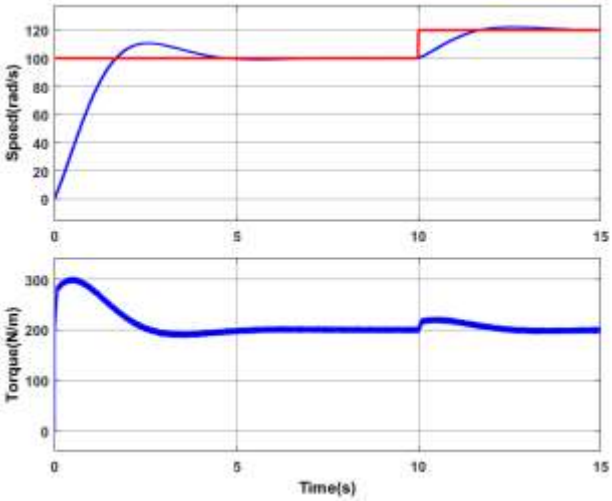

Fig. 17: Motor Speed and Torque

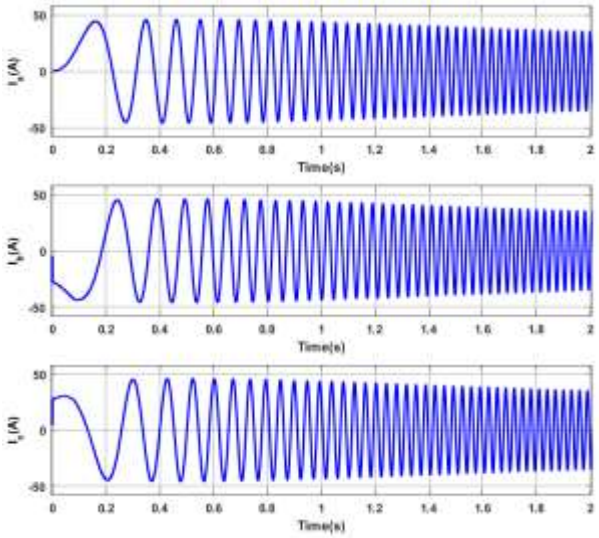

Fig. 18: Motor Stator Currents during Starting

CASE2: The performance of the proposed configuration of EV is investigated for variable irradiation in this case. Reference speed in vector control of vehicle drive is increased from 100 rad/sec to 120 rad/sec at 10 seconds. Irradiance is 600w/m^2 at starting increased to 800w/m^2 in the 3rd second increased to 1000 w/m^2 in the 6th second decreased to 400w/m2 in the 9th second and again increased to 900 w/m^2 in the 12th second. Variable irradiance is shown in Figure 19. PV and its boost converters output voltage, current, and power are shown in Figure 20 and Figure 21. Figure 22 and Figure 23 display the voltage, current, and power outputs of the fuel cell and its converters. Figure 24 and Figure 25 show the voltage, current, and power of the electrolyzer and its converters. Furthermore, the input voltage and boosted output voltage of the QBBC converter are shown in Figure 26. Due to the regulated and boosted output voltage of QBBC, the variance in irradiance of the PV cell does not affect the output voltage that is supplied to the vehicle drive inverter, as shown in Figure 27 where the motor speed and torque are displayed.

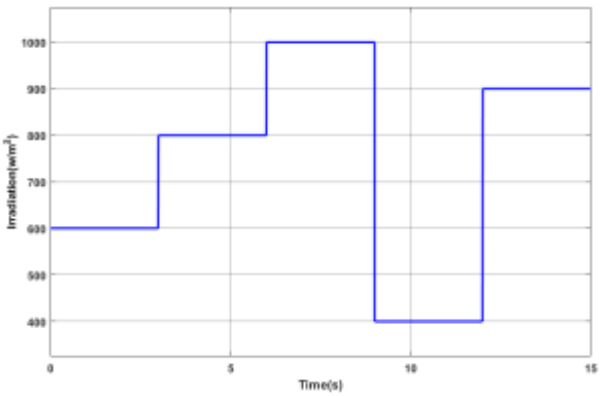

Fig. 19: Irradiance of PV cells

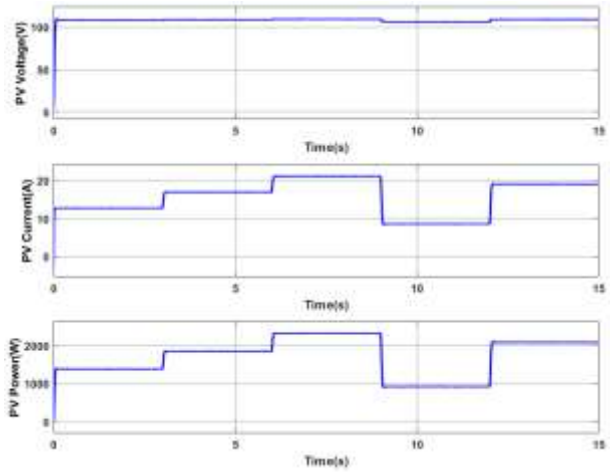

Fig. 20: PV array output voltage and power

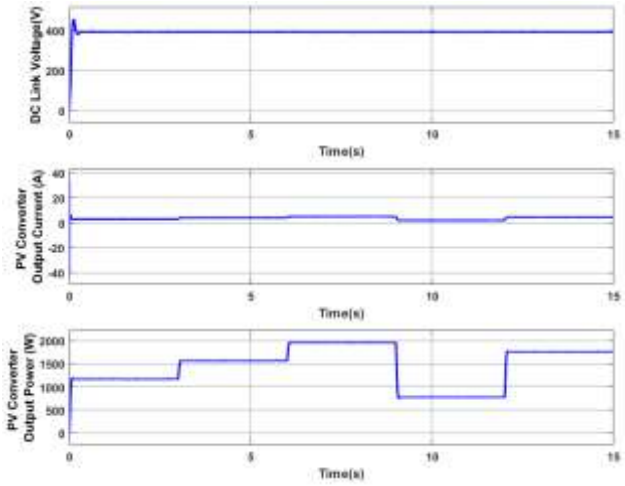

Fig. 21: PV converter output voltage, current, and power

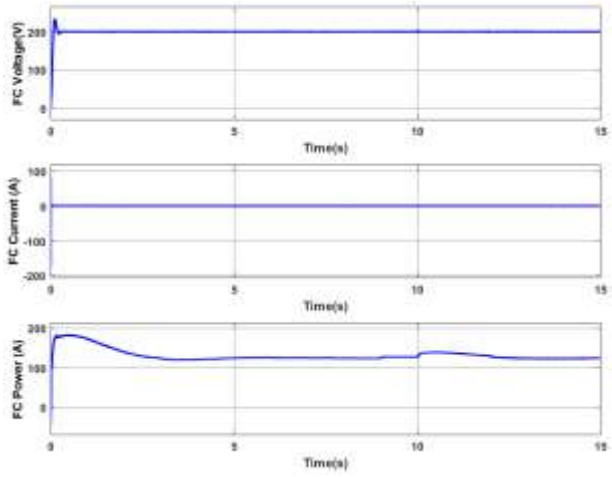

Fig. 22: Fuel Cell output voltage and power

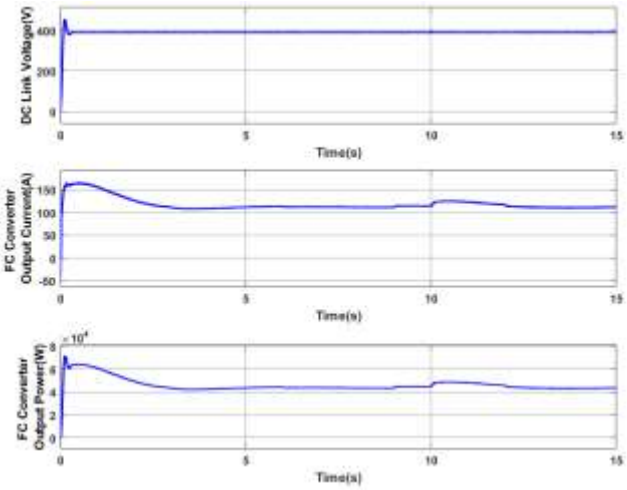

Fig. 23: FC converter output voltage, current, and power

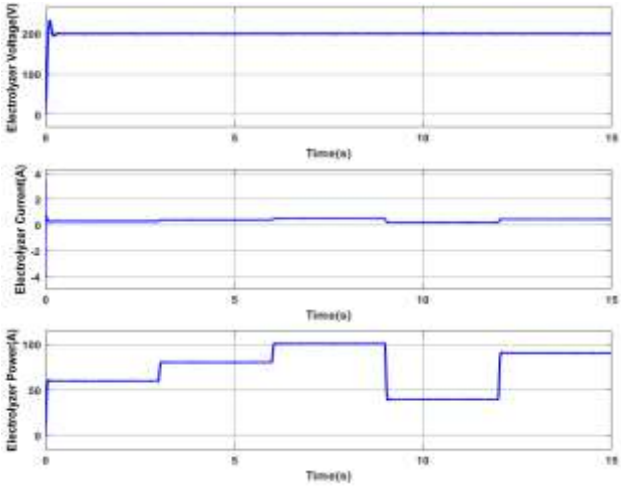

Fig. 24: Electrolyzer input voltage, current, and power

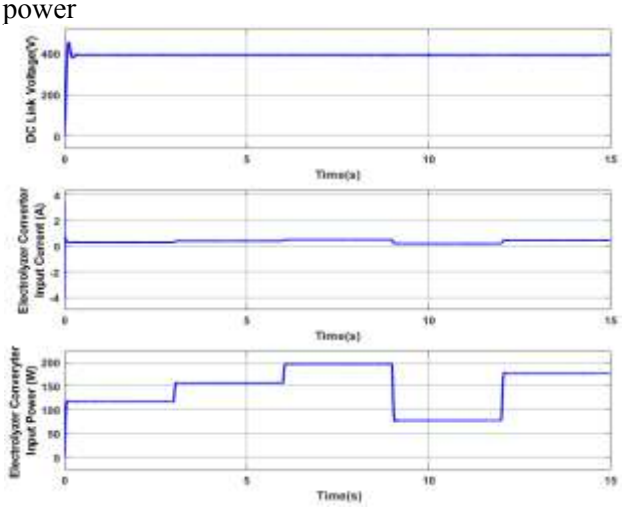

Fig. 25: Electrolyzer converter voltage, current, and power

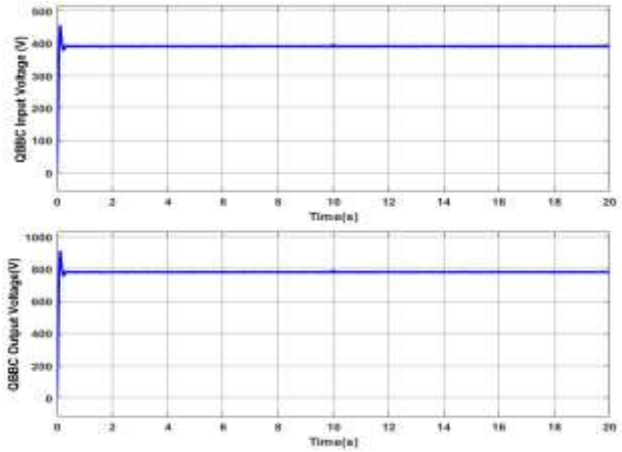

Fig. 26: QBBC input voltage and output voltage

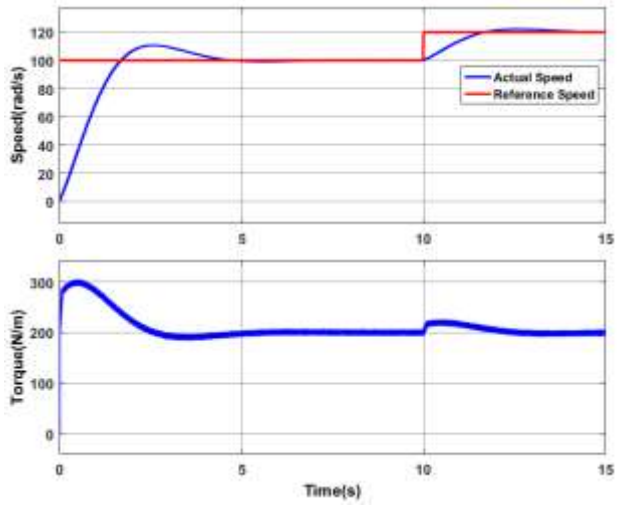

Fig. 27: Motor Speed and Torque

CASE 3: In this case, Irradiance is constant at 1000w/m^2. Speed is increased from 30rad/s to 50rad/s at 2.5 seconds then increased to 100rad/s at the 5th second then increased to 120rad/s at 7.5second then to 150rad/s at the 10th second then decreased to 100rad/s at 12.5second then decreased to 70rad/s at 15th second and decreased to 50rad/s at 17.5 seconds. The input and output voltage of QBBC is shown in Figure 28. The output voltage of the converter is regulated at 780V which is required by the vehicle drive inverter. Figure 29 depicts the motor speed and torque, while Figure 30 displays the output voltage, current, and power of the PV cell. Additionally, Figure 31 illustrates the output voltage, current, and power of the fuel cell. The motor's active and reactive power is shown in Figure 32.

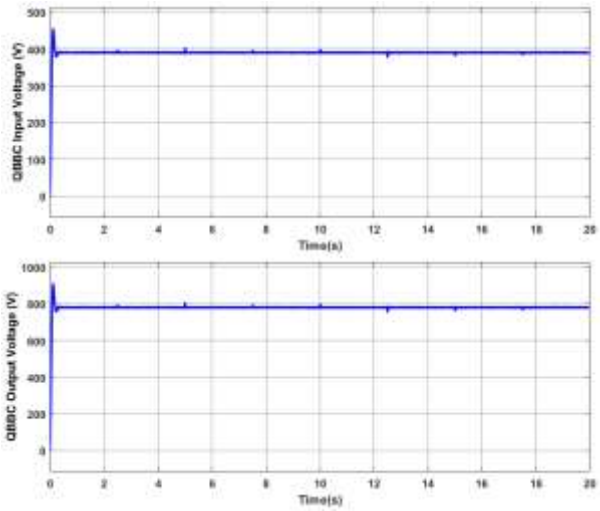

Fig. 28: QBBC input voltage and output voltage

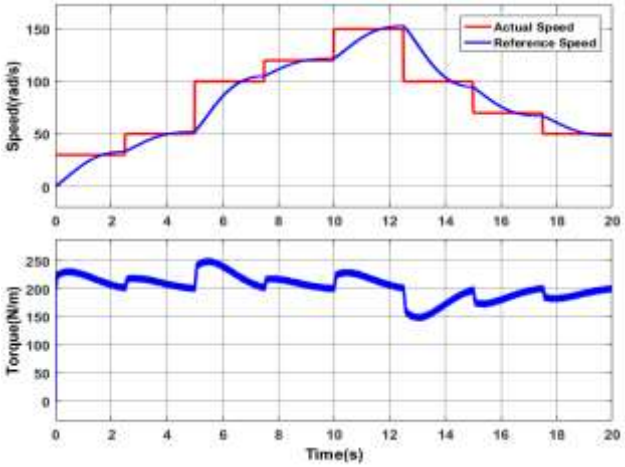

Fig. 29: Motor Speed and Torque

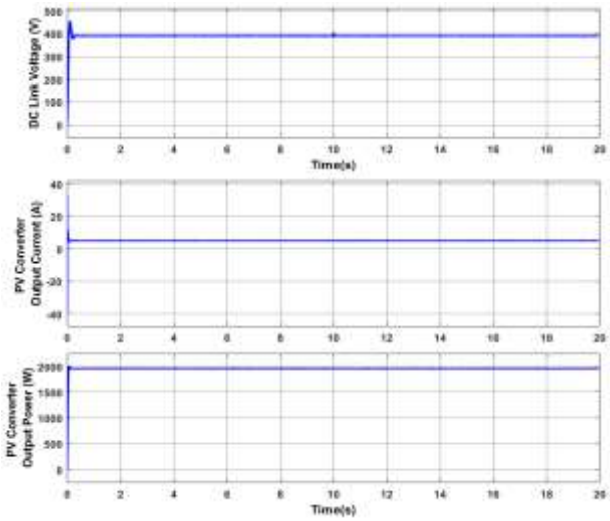

Fig. 30: PV converter output voltage, current, and power

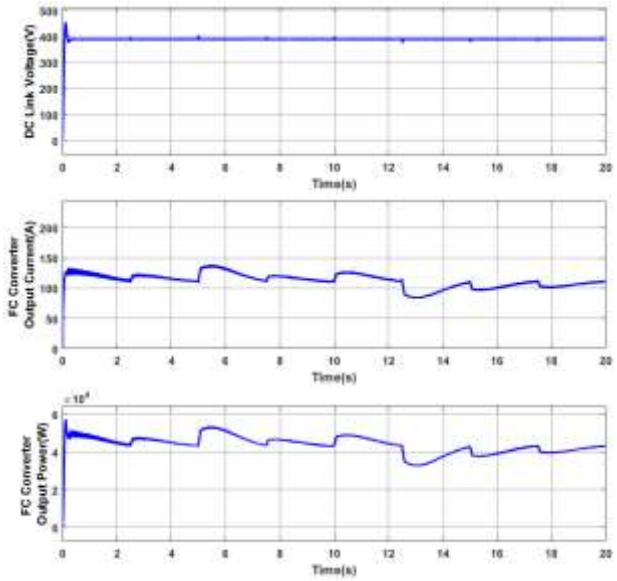

Fig. 31: FC converter output voltage, current, and power

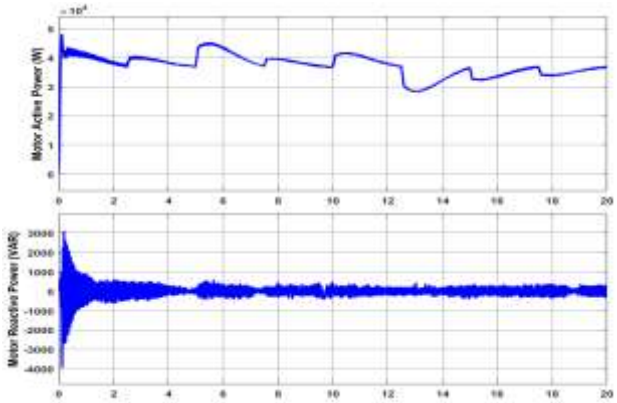

Fig. 32: Motor Input active and reactive power

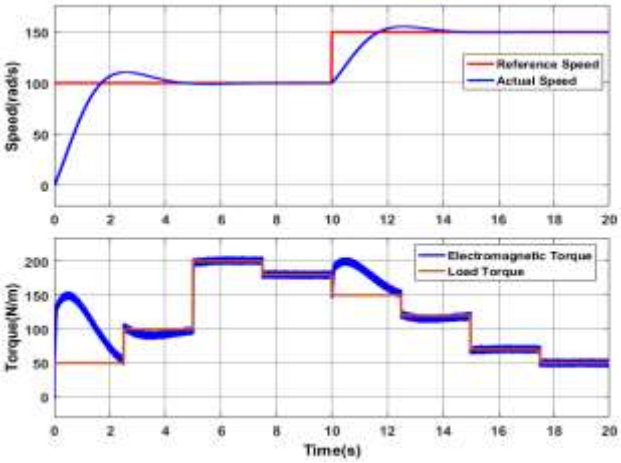

Fig. 33: Motor Speed and Torque

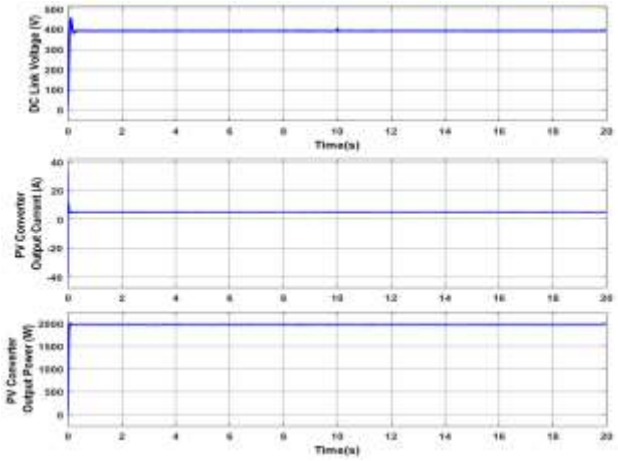

Fig. 34: PV converter output voltage, current, and power

CASE4: In this case, step changes in speed and variable load torque are considered. Reference speed is increased from 100 rad/sec to 150 rad/sec at 10 seconds. Load torque is increased from 50Nm to 100Nm at 2.5 seconds then increased again to 200Nm at the 5th second then decreased to 180Nm at 7.5second then to 150Nm at the 10th second then decreased to 120Nm at 12.5second then decreased to 70Nm at 15th second and decreased to 50Nm at 17.5 second. Vehicle drive speed and torque are shown in Figure 33. The output voltage, current, and power of the PV cell are shown in Figure 34. Figure 35 shows the output voltage, current, and power of the fuel cell, while Figure 36 displays the active and reactive power of the motor.

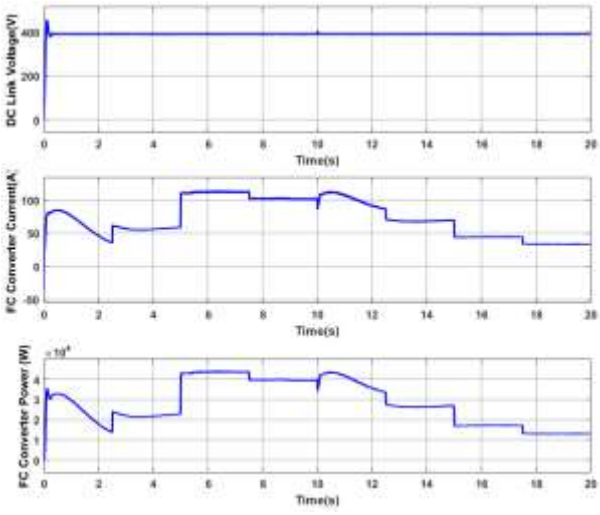

Fig. 35: FC converter output voltage, current and power

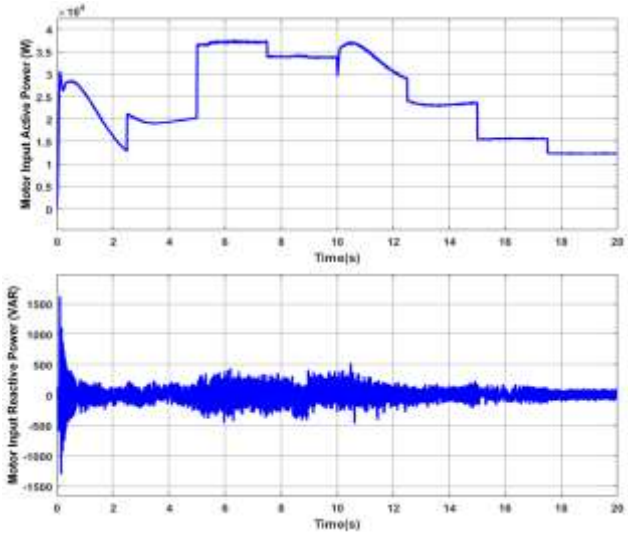

Fig. 36: Motor Input active and reactive power

5 Conclusion

The paper introduces a new electric vehicle (EV) configuration that incorporates a fuel cell, an electrolyzer, and an onboard PV cell, which is a novel concept. The onboard PV cell can help the fuel cell when there is sufficient irradiation to generate power. Moreover, an electrolyzer is employed to convert excess electric energy into chemical energy, which can be stored for later use. A quadratic bidirectional buck/boost converter is used to match the source voltage with the inverter DC side voltage of the vehicle drive. To extract the maximum available power from the PV panel, the system employs an incremental conductance Maximum Power Point Tracking (MPPT) algorithm to regulate the PV system. Outer voltage and inner current control loop are adopted for QBBC converter to regulate and boost up the voltage available at sources. To check the efficiency of the proposed configuration simulations are performed for changes in reference speed and change in irradiation. The simulation results presented represent efficient tracking of the reference speed of the motor. The efficiency of the proposed configuration is compared with conventional configuration and results are tabulated. By replacing the PI controller used in VCIMD with Model Predictive Control, the behavior of EV configuration can be evaluated with different driving cycles.

References:

[1] Ellingsen, Linda Ager- Wick, et al. "Life cycle assessment of a lithium- ion battery vehicle pack." Journal of Industrial Ecology 18.1 (2014): 113-124.

[2] Staffell, Iain, et al. "The role of hydrogen and fuel cells in the global energy system." Energy & Environmental Science 12.2 (2019): 463-491.

[3] Fathabadi, Hassan. "Novel fuel cell/battery/supercapacitor hybrid power source for fuel cell hybrid electric vehicles." Energy 143 (2018): 467-477.

[4] Thomas, C. E. "Fuel cell and battery electric vehicles compared." international journal of hydrogen energy 34.15 (2009): 6005-6020.

[5] Vyas, Anant D., Danilo J. Santini, and Larry R. Johnson. "Potential of plug-in hybrid electric vehicles to reduce petroleum use: Issues involved in developing reliable estimates." Transportation Research Record 2139.1 (2009): 55-63.

[6] Emadi, Ali, Young Joo Lee, and Kaushik Rajashekara. "Power electronics and motor drives in electric, hybrid electric, and plug-in hybrid electric vehicles." IEEE Transactions on industrial electronics 55.6 (2008): 2237-2245.

[7] Luo, Yang, et al. "Optimization and cutting- edge design of fuel- cell hybrid electric vehicles." International Journal of Energy Research 45.13 (2021): 18392-18423.

[8] Li, Huan, et al. "Online adaptive equivalent consumption minimization strategy for fuel cell hybrid electric vehicle considering power sources degradation." Energy Conversion and Management 192 (2019): 133-149.

[9] Offer, Gregory James, et al. "Comparative analysis of battery electric, hydrogen fuel cell, and hybrid vehicles in a future sustainable road transport system." Energy policy 38.1 (2010): 24-29.

[10] Jiao, Kui, et al. "Designing the next generation of proton-exchange membrane fuel cells." Nature 595.7867 (2021): 361-369.

[11] Trinh, Hoai-An, et al. "Comprehensive Control Strategy and Verification for PEM Fuel Cell/Battery/Supercapacitor Hybrid Power Source." International Journal of Precision Engineering and Manufacturing-Green Technology (2022): 1-16.

[12] Do, Tri Cuong, et al. "Energy management strategy of a PEM fuel cell excavator with a supercapacitor/battery hybrid power source." Energies 12.22 (2019): 4362.

[13] Pukrushpan, J.P.; Stefanopoulou, A.G.; Peng, H. Control of Fuel Cell Power Systems: Principles, Modeling, Analysis and Feedback Design; Springer: London, UK, 2004.

[14] Lakshmi, P. Naga, R. Ashok Kumar, and K. Hari Krishna. "DC-DC converter in microgrid for voltage regulation and ripple reduction using electric spring technology" International Journal of Power and Energy Systems 42.10 (2022).
[15] Pires, Vitor Fernão, Daniel Foito, and Armando Cordeiro. "A DC–DC converter with quadratic gain and bidirectional capability for batteries/supercapacitors." IEEE Transactions on Industry Applications 54.1 (2017): 274-285.

Contribution of Individual Authors to the Creation of a Scientific Article (Ghostwriting Policy)
The authors equally contributed to the present research, at all stages from the formulation of the problem to the final findings and solution.

Sources of Funding for Research Presented in a Scientific Article or Scientific Article Itself
No funding was received for conducting this study.

Conflict of Interest
The authors have no conflicts of interest to declare.

Creative Commons Attribution License 4.0 (Attribution 4.0 International, CC BY 4.0)
This article is published under the terms of the Creative Commons Attribution License 4.0
https://creativecommons.org/licenses/by/4.0/deed.en_US